Highly deformable bones: Unusual deformation mechanisms of seahorse armor

Michael M. Porter [a,*], Ekaterina Novitskaya [a], Ana Bertha Castro-Ceseña [a,1], Marc A. Meyers [a,b,c], Joanna McKittrick [a,b]

[a] Materials Science and Engineering Program, University of California, San Diego, 9500 Gilman Drive, La Jolla, CA 92093, USA
[b] Department of Mechanical and Aerospace Engineering, University of California, San Diego, 9500 Gilman Drive, La Jolla, CA 92093, USA
[c] Department of NanoEngineering, University of California, San Diego, 9500 Gilman Drive, La Jolla, CA 92093, USA

ARTICLE INFO

ABSTRACT

Multifunctional materials and devices found in nature serve as inspiration for advanced synthetic materials, structures and robotics. Here, we elucidate the architecture and unusual deformation mechanisms of seahorse tails that provide prehension as well as protection against predators. The seahorse tail is composed of subdermal bony plates arranged in articulating ring-like segments that overlap for controlled ventral bending and twisting. The bony plates are highly deformable materials designed to slide past one another and buckle when compressed. This complex plate and segment motion, along with the unique hardness distribution and structural hierarchy of each plate, provide seahorses with joint flexibility while shielding them against impact and crushing. Mimicking seahorse armor may lead to novel bioinspired technologies, such as flexible armor, fracture-resistant structures or prehensile robotics.

1. Introduction

Recent interest in biomimicry and bio-inspired design has led to a renewed study of biological materials and devices [1,2]. Nature offers a plethora of functional designs, ranging from spider silk to insect flight, that inspire materials scientists and engineers to develop new, high-performance materials, structures and robotic devices [2–6]. In a quest to discover novel, multifunctional defense mechanisms that exist in nature, we investigated the structure–property–function relationships of the bony-plated armor in the seahorse, *Hippocampus kuda*.

Seahorses, known for their equine profile and vertical swimming posture, are remarkable fish with a variety of characteristics unique to the genus *Hippocampus*, family Syngnathidae. They have a head like a horse, a long tubular snout like an anteater, eyes that move independently like a chameleon, a brood pouch like a kangaroo, camouflage skin like a flounder, and a flexible prehensile tail like a monkey [7,8]. Unlike most fish, seahorses have no caudal fin and swim upright with a single dorsal fin for propulsion and two pectoral fins for maneuverability [9,10]. This unique posture, their cryptic appearance, and their ability to suction feed and grasp objects allow these slow swimmers to thrive in obstacle-strewn

sea grasses, mangroves and coral reefs [7,8]. Although seahorses primarily rely on camouflage skin and dermal excrescences (e.g. filamentous or polyp-like growths) to avoid predators [7,8], they have evolved a segmented array of bony plates that functions as a flexible, subdermal armor [11,12]. This armor serves as protection against compressive failure, as several of their natural predators, including larger fish, crabs, rays, sea turtles and birds, capture their prey by crushing [13].

Natural armor in most marine animals, such as bony fish, crustaceans, and molluscs, often exists in the form of external scales, exoskeletons and shells [14–16]. These natural materials are typically rigid, mineralized structures designed for body support and environmental protection [14–16]. Seahorses, in contrast to most teleosts, have internal bony plates instead of scales, arranged in articulating ring-like segments spanning the length of the fish. The bony plates not only provide seahorses with body support and protection, but also give them the ability to bend their tails to grasp and hold objects [11,12].

Most natural armor in fish limits axial bending [17,18]—a necessary tradeoff for the protection it provides. However, Hale [11] and Praet et al. [12] argue that the bony plates in seahorses play an essential role in axial bending and the prehensility of their tails. In fact, seahorses can precisely control body movements to twist and bend ventrally—motions usually disadvantageous in laterally swimming fish [11]. The body plating provides a rigid structure for myomere muscles to pull on and transmit forces to the vertebrae [11,12]. In the tail, the hypaxial muscles are oriented

---

vertically, connecting the ventral plates to the horizontal septa of the vertebrae, while the epaxial muscles are oriented concentrically, connecting the dorsal plates to the vertebrae [12]. This is very different from most teleosts, whose muscles are all oriented concentrically and pull directly on the vertebrae, with thick collagen fibers in the skin that limit body twisting and ventral bending [11,17,19]. Beyond muscular force transmission and body mobility, the bony plates play a defensive role as protective armor. The bony armor must be mechanically hard and sufficiently tough to resist fracture from impact and crushing, yet elastic and flexible enough for controlled axial bending and prehension.

The mechanisms of plate and segment motion, the structural hierarchy and the mechanical properties of the bony-plated armor that protect seahorses are revealed here through microcomputed tomography (μCT), scanning electron microscopy (SEM) and mechanical testing. The overlapping architectural arrangement of the bony plates and segments are shown to allow significant deformations without fracture, protecting the spinal column from catastrophic failure. The material composition, microstructural features and hardness of the bony plates are investigated and compared to that of other natural materials, including fish scales, crab exoskeleton, abalone nacre and bovine femur bone. Mimicking the multifunctional bony-plated armor of the seahorse tail may lead to new bio-inspired technologies.

2. Materials and methods

2.1. Sample collection and preparation

Eight mature and three juvenile seahorse specimens of *H. kuda* were donated by the Birch Aquarium at the Scripps Institute of Oceanography, University of California, San Diego, on October 2011. The seahorses were confiscated alive in Bali, Indonesia on October 2005 and died, due to stress, during transport to the aquarium, where they were subsequently kept frozen. The specimens were thawed and preserved by immersing them in 70% isopropanol at room temperature, rather than physiological solution, to prevent degradation of the specimens during analysis.

2.2. Material composition

The water, mineral and organic fractions of the seahorse bones were measured by weight. Six bony plates were excised from the base (torso–tail intersection) of a mature seahorse tail. The bony plates were thoroughly cleaned under an optical microscope using tweezers to remove and scrape away any connective tissue and skin. Any remaining organic material left on the bones was small and considered negligible. To rehydrate the cleaned bones, the samples were submerged in Hank's balanced saline solution for 24 h. The water content was determined by heating the bones in an oven at 105 °C for 4 h to dehydrate them. The mineral (ash) content was determined by subsequent heating in an oven at 550 °C for 24 h to eliminate the organic content. The weights of the individual samples were measured before and after the heating processes. The water, mineral and organic fractions of the bony plates were calculated using the following equations:

$$x_{\text{water}} = \left(1 - \frac{m_{\text{dry}}}{m_{\text{wet}}}\right) \times 100\% \tag{1}$$

$$x_{\text{mineral}} = \left(\frac{m_{\text{ash}}}{m_{\text{wet}}}\right) \times 100\% \tag{2}$$

$$x_{\text{organic}} = \left(\frac{m_{\text{dry}} - m_{\text{ash}}}{m_{\text{wet}}}\right) \times 100\%, \tag{3}$$

where x_i is the wt.% of component i—water, mineral and organic— and m_j is the measured mass of component j—hydrated (wet) sample, dehydrated (dry) sample and mineral (ash) sample, respectively.

2.3. Deproteinization

To visualize the overlapping sequence of the subdermal bony plates, partial deproteinization was carried out to remove the skin. Two mature seahorse tails were fully submerged in a 12.5% NaClO solution for 30 min, then rinsed with deionized water and dried in a desiccant at room temperature for 2–3 days. The partial deproteinization process was effective in dissolving the outermost layer of organic material (i.e. skin). With the skin removed, the architecture and assembly of the overlapping bony plates could be more easily visualized and studied.
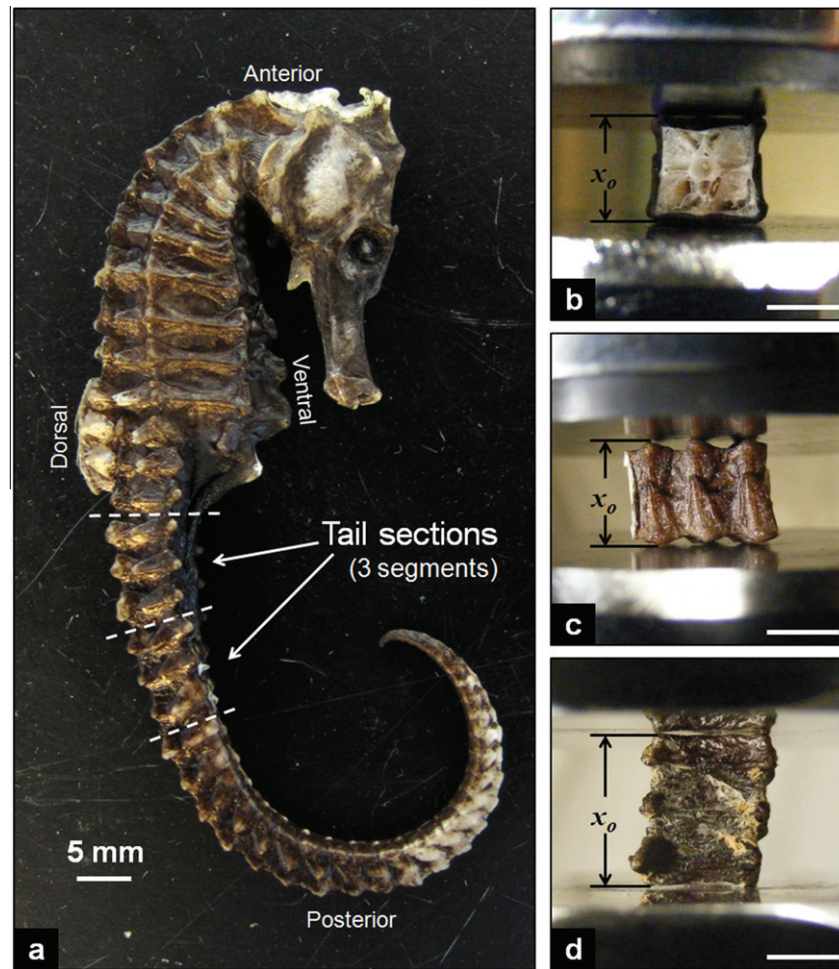
2.4. Compression testing

Six tail sections cut from the base (torso–tail intersection) of three mature seahorse tails, containing three bony segments per tail section, were cut and loaded in compression with an Instron materials testing machine (Instron 3367, Norwood, MA) with a 30 kN load cell at a cross-head velocity of 10^{-3} mm s^{-1}. The tail sections were compressed to a displacement of ~60% of the original specimen height (x_0) in one of three orthogonal directions: (i) lateral; (ii) ventral–dorsal; (iii) distal–proximal. Two tail sections were compressed in each direction. Each tail section was placed between the cross-heads freely, such that the edges were not restricted and allowed to reorient under the compressive load. Fig. 1 illustrates the locations where the tail sections were cut from the seahorse (Fig. 1a) and the positioning of the tail sections in the Instron machine before compression (Fig. 1b–d). The specimens were preserved in 70% isopropanol until tested; then they were removed, immediately placed on the compression testing platform, and compressed. To ensure the specimens remained saturated, the samples were quenched every 1–2 min with 70% isopropanol using a squirt bottle. The measured dimensions of the tail sections were approximately $7 \times 7 \times 10$ mm^3. Representative force–displacement curves were plotted for comparison. The percent displacement, analogous to the total body strain, was plotted to account for differences in the initial heights of the different orientations of the tail sections, calculated from the following equation:

$$\% \text{ displacement} = \frac{x}{x_0} \times 100\%, \tag{4}$$

where x_0 is the initial height of the tail section and x is the measured displacement of the tail section, which was measured with an Epsilon deflectometer (Epsilon 3540, Jackson, WY). After compression of each tail section in one of the three orthogonal directions, each compressed specimen was removed from the Instron machine and dried in a desiccant at room temperature for 2–3 days for imaging and further analysis.

2.5. Microhardness testing

The microhardness of the bony plates was measured using a LECO M-400-H1 hardness testing machine equipped with a Vickers hardness indenter. Four dorsal plates excised from two tail segments cut from the base (torso–tail intersection) of a mature seahorse tail were cleaned, dried in a desiccant at room temperature for 2–3 days, embedded in epoxy resin and polished until the surfaces of the samples were exposed. The embedded bony plates were positioned such that four different locations of each plate could be tested to determine the overall hardness distribution across a single bony plate. Hardness values at the four different locations were averaged from 16 microindentations each. The surface hardness of several bony plates along the length of the tail was

Fig. 1. (a) Image of a mature seahorse (*Hippocampus kuda*) showing the locations where tail sections, composed of three bony segments each, were cut (dotted lines) for compression testing. (b–d) Images of the positioning of the tail sections in the Instron machine before compression: (b) ventral–dorsal loading, distal view; (c) ventral–dorsal loading, lateral view; (d) distal–proximal loading, lateral view. *Note:* Positioning of the tail sections for lateral loading is similar to ventral–dorsal loading. The initial specimen height (cross-head distance) is denoted as x_0. Scale bars: 5 mm.

also measured to confirm that the hardness remained constant along the length. The hardness of the interior and exterior of several bony plate cross-sections (10 indentations each) were also measured. A load of 0.981 N was used to indent the exposed surfaces. The Vickers hardness of the bony plates was evaluated using the following equation:

$$HV = \left(1.854 \frac{F}{d^2}\right) \tag{5}$$

where HV is the Vickers hardness number (MPa), F is the applied load (N) and d is the arithmetic mean of the two measured diagonals (mm).

For comparison, the microhardness of dry *Arapaima gigas* fish scales, a crab exoskeleton, abalone nacre and cortical bovine femur bone were also measured and compared to values reported in the literature [14–16,20,21]. The microhardnesses of the different samples was averaged from 10 to 20 indentations each at a load of 0.981 N. Table 1 compares the measured hardness values with those reported in the literature.

2.6. Microcomputed tomography

The following samples were scanned on a Skyscan 1076 μCT scanner (Kontich, Belgium): (i) a juvenile seahorse, ∼6 months old, immersed in 70% isopropanol to prevent shrinkage due to

Table 1
Comparison of the measured microhardness with the hardness reported in the literature for mature seahorse bony plates, *Arapaima gigas* fish scales, crab exoskeleton, abalone nacre and bovine femur bone.

|	Hardness (MPa)	Indent load (N)	References
Seahorse bony plates			
Measured	80–320	0.981	This work
Arapaima gigas fish scales			
Measured	270 ± 20	0.981	This work
Literature	100–600	0.245	[14]
Crab exoskeleton			
Measured	250 ± 70	0.981	This work
Literature	250–950	0.245	[15]
Abalone nacre			
Measured	3080 ± 440	0.981	This work
Literature[a]	500–3000	0.1–1.6 mN	[16]
Bovine femur bone			
Measured	680 ± 70	0.981	This work
Literature	550–700	0.491	[20,21]

[a] Hardness values of abalone nacre reported in the literature were measured via nanoindentation experiments.

dehydration; (ii) a dried tail section composed of three bony-plated segments; (iii) three different tail sections (three segments each) compressed in different orthogonal directions (refer to Fig. 1 and Section 2.4) and dried; and (iv) a dried bony plate excised from the left dorsal side of a mature seahorse tail. A juvenile seahorse
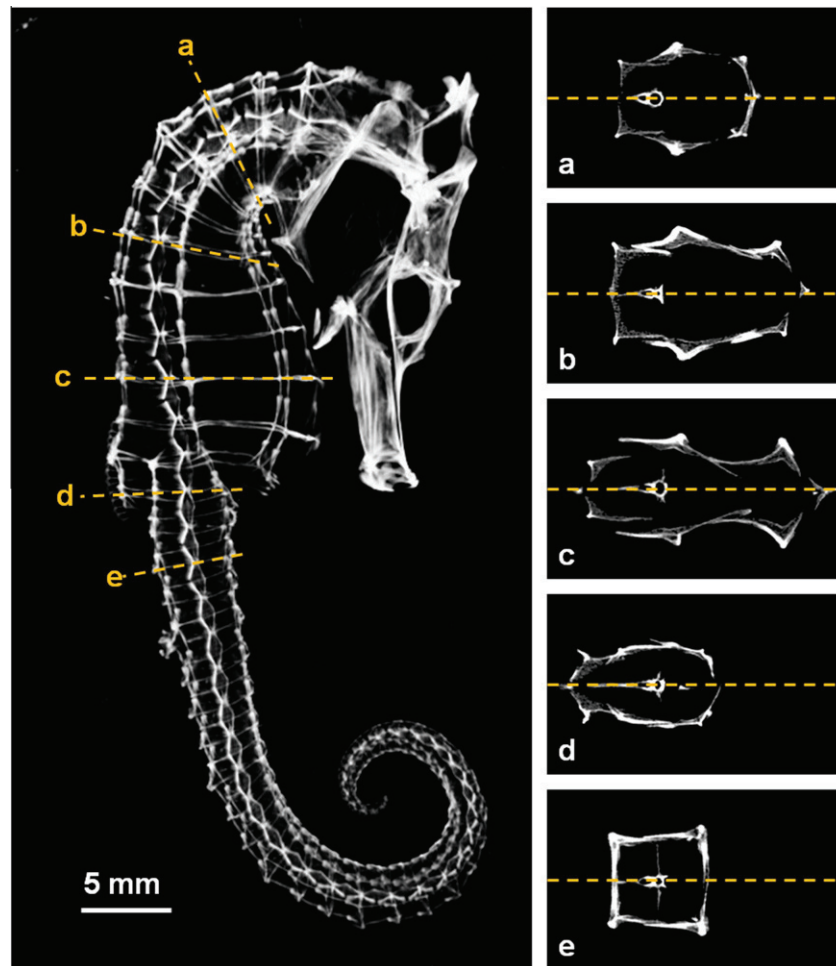
Fig. 2. µCT scan of a juvenile seahorse skeleton (*Hippocampus kuda*) illustrating the cross-sections of several different segments along the length of the fish: (a–c) heptagonal segments at different locations of the torso; (d) hexagonal segment at the dorsal fin (torso–tail intersection); (e) square-like segment of the prehensile tail.
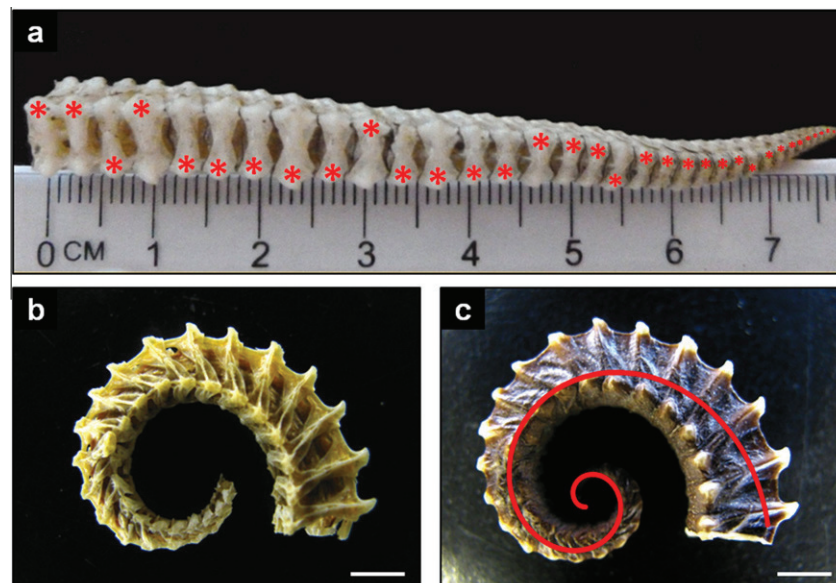
**Fig. 3.** Images of mature seahorse tails illustrating: (a) the random lateral overlap sequence of the dorsal plates along the length of the tail—red asterisks indicate the top overlapping plates of each segment; (b) the ventral–dorsal and distal–proximal overlaps of the plates; (c) a superimposed logarithmic spiral. (a,b) Tails were partially deproteinated with 12.5% NaClO for 30 min to remove the skin. Scale bars: 5 mm.
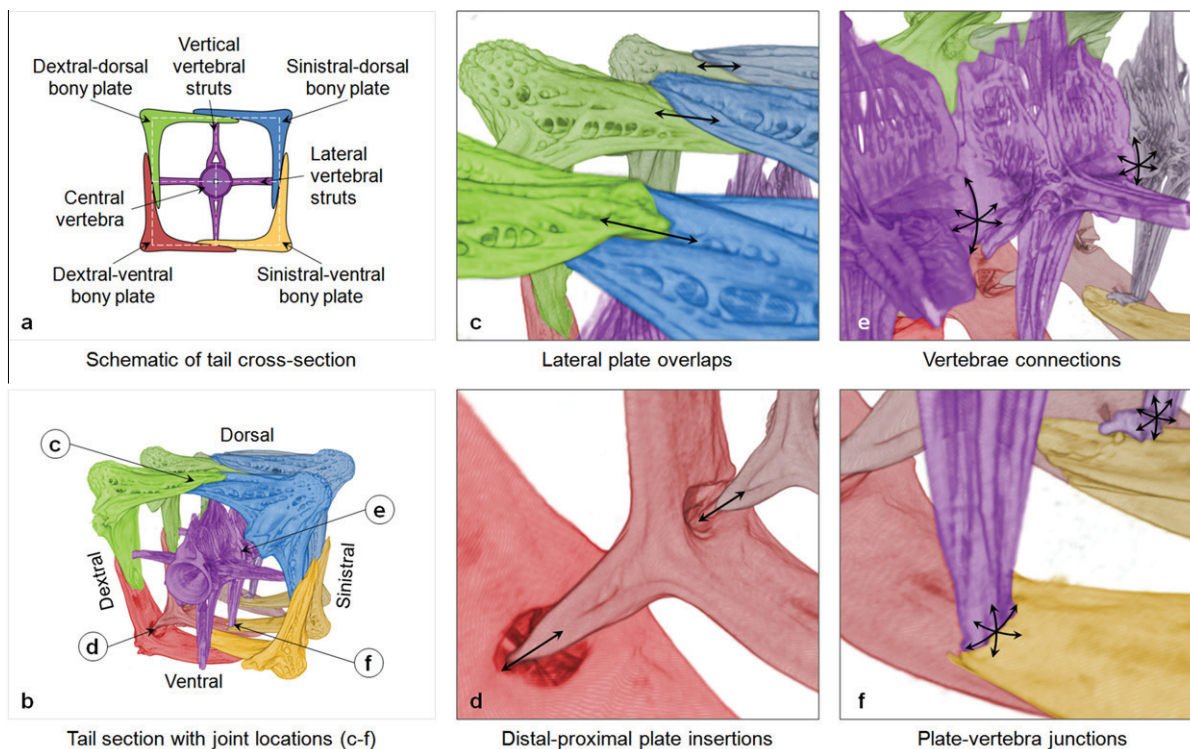
Fig. 4. (a) Schematic of a seahorse tail cross-section (distal view), denoting each bony plate and vertebra components; (b) μCT image of a mature seahorse tail section (three bony segments) illustrating the four different joints: (c) lateral plate overlaps and gliding joints; (d) distal–proximal plate insertions and gliding joints; (e) vertebrae connections and pivoting joints; (f) plate–vertebra junctions and pivoting joints. Arrows indicate the directions of translational (gliding) (c and d) and rotational (pivoting) (e and f) degrees of freedom. All μCT images were colored for clarity with Jasc Paint Shop Pro.

was imaged instead of a mature seahorse to reduce the scan and image reconstruction time. For sample preparation, the seahorse was wrapped in a Kimwipe tissue moistened with a phosphate buffer saline solution and placed in a sealed tube to prevent the specimen from drying out during scanning. The four tail sections and the bony plate were scanned inside dry plastic tubes. The seahorse

was scanned with an isotropic voxel size of 36 μm, a rotation step of 0.7° and an exposure time of 80 ms. The four tail sections were scanned with an isotropic voxel size of 9 μm, a rotation step of 0.8° and an exposure time of 1650 ms. The bony plate was scanned with an isotropic voxel size of 9 μm, a rotation step of 0.7° and an exposure time of 1650 ms. An electric potential of 70 kV and a
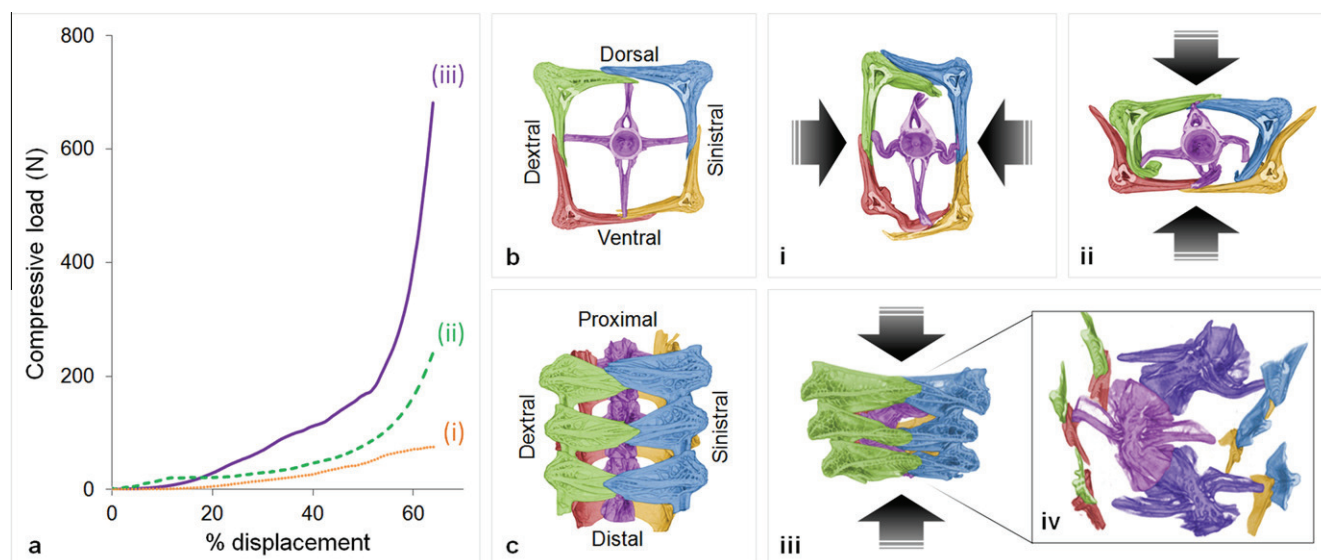
Fig. 5. (a) Force–displacement curves of three different mature seahorse tail sections (three bony segments each) compressed to ∼60% displacement: (i) laterally (dextral–sinistrally), (ii) ventral–dorsally and (iii) distal–proximally. μCT images: (b) distal view of tail cross-section before compression; (c) dorsal view of tail section before compression; (i) distal view of tail cross-section compressed laterally; (ii) distal view of tail cross-section compressed ventral–dorsally; (iii) dorsal view of tail section compressed distal–proximally; (iv) magnified cutaway of image (iii) showing vertebrae bending due to distal–proximal loading. All samples were compressed to a displacement ∼60% of the original sample height. All μCT images were colored for clarity with Jasc Paint Shop Pro.

current of 200 μA were applied using a 0.5 mm aluminum filter during all scans. A beam-hardening correction algorithm was applied during image reconstruction of all samples. Images and three-dimensional rendered models were developed using Skyscan's Dataviewer and CTVox software.

2.7. Scanning electron microscopy

Prior to imaging the bones were cleaned under an optical microscope, washed with deionized water, then dried in a desiccant for 48 h and sputter-coated with iridium using an Emitech K575X sputter coater (Quorum Technologies Ltd., West Sussex, UK). Both fully intact and fracture surfaces of the specimens were imaged at 5 kV with a Philips XL30 field emission environmental scanning electron microscope (ESEM) (FEI-XL30, FEI Company, Hillsboro, OR). Energy-dispersive X-ray spectroscopy (EDX) was performed with the ESEM on uncoated specimens using an Oxford EDX attachment and Inca software for elemental analysis.

3. Results and discussion

3.1. Seahorse anatomy

Fig. 2 shows μCT images of a juvenile seahorse skeleton (H. kuda), illustrating the morphology of several ring-like segments, each composed of plates surrounding a single vertebra, at different locations along the fish. The torso is supported by a scaffold of ~11 heptagonal segments (Fig. 2a–c). At the dorsal fin (torso–tail intersection) the segments become hexagonal (Fig. 2d), and then square (Fig. 2e). The prehensile tail has ~36 square-like segments (Fig. 2e), each composed of four corner plates that decrease linearly in size along the length of the tail as seen in Fig. 3a. The plates and vertebrae are joined by thick, subdermal collagen layers of connective tissue and free to glide or pivot depending on the particular design of each joint. Praet et al. [12] identified eight gliding joints and five pivoting (ball-and-socket) joints per tail segment. Gliding joints are composed of bones that can slide past one another with one degree of translational freedom, while pivoting joints allow rotation, much like a ball-and-socket joint, with three degrees of rotational freedom [12].

Fig. 4 shows the architectural arrangement of the different bones (Fig. 4a) and joints (Fig. 4b) in the tail. Adjacent bony plates in each tail segment overlap at the dorsal, ventral and lateral midlines (Fig. 4c) [11,12]. There are four gliding joints per segment with this configuration. On both the dextral and sinistral sides of the tail, the ventral plates always overlap the dorsal plates as seen in Fig. 3b [12]. Conversely, the dextral–sinistral or sinistral–dextral overlaps on the dorsal and ventral sides of the tail are randomly sequenced from segment to segment as shown in Fig. 3a, and may be distinct to each individual seahorse, much like the uniqueness of their cranial coronets [7]. Each ring of bony plates overlaps its anterior neighbor to permit axial bending (see Fig. 3b). Neighboring segments are connected by four gliding joints where the distal spines of the anterior plates insert into the proximal grooves of the posterior plates (Fig. 4d) [11,12]. Even though the soft connective tissue provides these joints with some rotational and translational freedom, the gliding motion of the plates is predominantly restricted to one translational degree of freedom (see arrows in Fig. 4c and d). Successive vertebrae, on the other hand, are connected by pivoting joints with three rotational degrees of freedom (Fig. 4e) [12]. Each vertebra is joined to the bony plates by connective tissue attached to the vertebral struts at the dorsal, ventral and lateral midlines (Fig. 4f) [12]. The plate–vertebra junctions are extremely flexible joints with nearly six degrees of freedom: three rotational (pivoting) and three translational (gliding)—although

translational motion is fairly limited [12]. This complex mechanism of plate and segment motion, regulated by collagenous connective tissue, allows seahorses to bend their tails ventrally in a logarithmic spiral (Fig. 3c) [22]. Slight lateral bending can occur concurrently with ventral bending; however, the regular ventral–dorsal overlaps and random lateral overlaps seem to prevent significant lateral bending [11].

3.2. Tail deformation mechanisms

Fig. 5 contains results from compression tests on seahorse tail sections, composed of three bony segments each (refer to Fig. 1). The tail sections were compressed to a displacement of ~60% of the original specimen height in one of three orthogonal directions: (i) lateral (dextral–sinistral), (ii) ventral–dorsal and (iii) distal–proximal. As seen in the load–displacement plot (Fig. 5a), the tail exhibits an anisotropic response to compressive loading, suggesting that the three-dimensional geometry and architecture of the tail influences the directionally dependent responses to compressive loading.

Fig. 5b and c show μCT images of the distal and dorsal views of a seahorse tail section before compression. When compressed laterally (Fig. 5i), the tail undergoes large deformations caused by relatively small forces, with the connective tissue and muscles bearing the load. At ~60% displacement, the lateral struts deform by local buckling, allowing the bony plates to slide past each other with relative ease. Once the plates reach the terminal corner of its lateral neighbor, they too begin to buckle (see dextral–ventral plate (red) in Fig. 5i). When compressed ventral–dorsally, the compressive loading rise rate is slightly greater than in lateral compression (see Fig. 5a). In this direction (Fig. 5ii), the vertical struts buckle and the lateral struts bend downward in the direction of the sliding dorsal plates. The ventral plates slide over the dorsal plates and fan out, while the dorsal plates slide under the ventral plates and buckle-in upon ventral–dorsal loading (see Fig. 5ii). There are two mechanisms that may add strength to the tail in the ventral–dorsal direction: (i) the vertical struts of the vertebrae are larger and more robust than the lateral struts; and (ii) the vertical orientation of the hypaxial muscles may resist deformation when loaded parallel to the myomere orientation. Compression of the seahorse tail in the lateral and ventral–dorsal directions does not result in brittle fracture, unlike many bony structures. Rather, the sliding motion of the bony plates, with most of the deformation being accommodated by the extension of connective collagen fibers, protects the spinal column from permanent damage.

Fig. 5iii and iv show the dorsal view of the bony plates and vertebrae of a tail section compressed distal–proximally. The strength of the tail section at ~60% displacement in this direction is nearly three times the strength in the ventral–dorsal direction (see Fig. 5a). Fig. 5iii shows the anterior plates sliding into the posterior plates. When compressed distal–proximally, the distal spines of the anterior plates do not deform, but slide beyond the proximal grooves of the posterior plates (refer to Fig. 4d). Instead, the vertebrae seem to bear the majority of the load and bend in response to the distal–proximal loading. As seen in Fig. 5iv, the lateral vertebral struts detach from the bony plates on one side of the tail and buckle on the opposing side.

3.3. Bony plate material properties

In addition to the multicomponent tail structure detailed in Figs. 3–5, the bony plates themselves are highly deformable materials. The bony plates are inorganic/organic composites composed of approximately 40 ± 5 wt.% mineral (calcium phosphate), 27 ± 4 wt.% organic (including proteins and <3 wt.% lipids [23]), and 33 ± 5 wt.% water, with an average microhardness of

Table 2
Comparison of the mineral, organic and water content in mature seahorse bony plates and bovine femur bone.

	Mineral (wt.%)	Organic (wt.%)	Water (wt.%)	References
Seahorse bony plates	40 ± 5	27 ± 4	33 ± 5	This work
Bovine femur bone	65	25	10	[20,21]

230 ± 80 MPa, which is constant along the length of the tail. Compared to bovine femur bone, composed of ~65 wt.% mineral [20,21] and a hardness ranging from 550 to 700 MPa [20,21], seahorse bones have a lower mineral content and hardness. This results in highly deformable bones that can withstand large deformations without fracture. Table 2 compares the mineral, organic and water content of the bony plates with that of bovine femur bone.

To withstand failure from impact, the bony-plated armor must be sufficiently hard. For comparison, the hardness of the armored fish *A. gigas* fish scales, crab exoskeleton and abalone nacre are 100–600 MPa [14], 250–950 MPa [15] and 500–3000 MPa [16], respectively (see Table 1). Fig. 6 (center) shows the Vickers hardness distribution across different structural features of a single bony plate. The proximal groove (160 ± 50 MPa) is nearly 40% softer than the distal spine (260 ± 40 MPa), enabling it to absorb the stresses associated with joint movement. Accordingly, the micrographs in Fig. 6a and b show that the proximal groove is porous, which may help dampen joint movement during prehensile

activities. The ridge nodules on the outer tip of the bony plates are the hardest region of the bone (320 ± 30 MPa) and may function as a hard, protective shield against high impact. The plate wings have an average hardness of 230 ± 50 MPa. The surface morphologies of the plate wings vary depending on whether the plate is on the outer or inner side of the plate–plate overlap (refer to Figs. 3a,b and 4c). The outer plate wing is supported by a single solid rod-like strut (Fig. 6c). The strut on the inner plate wing becomes branched into two or more smaller struts at the tip to provide structural reinforcement and a wider surface area for plate–plate attachment (Fig. 6d).

The micrographs shown in Fig. 6e–g reveal the structural hierarchy of a bony plate. The plates have hollow microchannels (100–500 μm in diameter) running the length of each plate wing and the distal spine that connect to a central hollow chamber beneath the ridge nodules (see Fig. 6e). External layers of harder mineralized tissue (160–320 MPa) encase a softer interior (80–200 MPa) that surrounds the hollow core. This type of structural gradient is similarly observed in other mineralized biological composites, such as fish bones, mammalian bones, teeth and antlers [24,25]. Local collapse of the hollow interior due to compressive loading may help protect the overall tail structure from damage. Additionally, the hollowness reduces weight while maintaining bending resistance. Examination of several different cross-sections of the bony plates revealed that the bones are acellular, showing no evidence of osteocyte lacunae in the internal structure [25]. A fracture surface of the distal spine (Fig. 6f) shows the orientation of structural fibers that surround microtubules (1–5 μm in diameter)
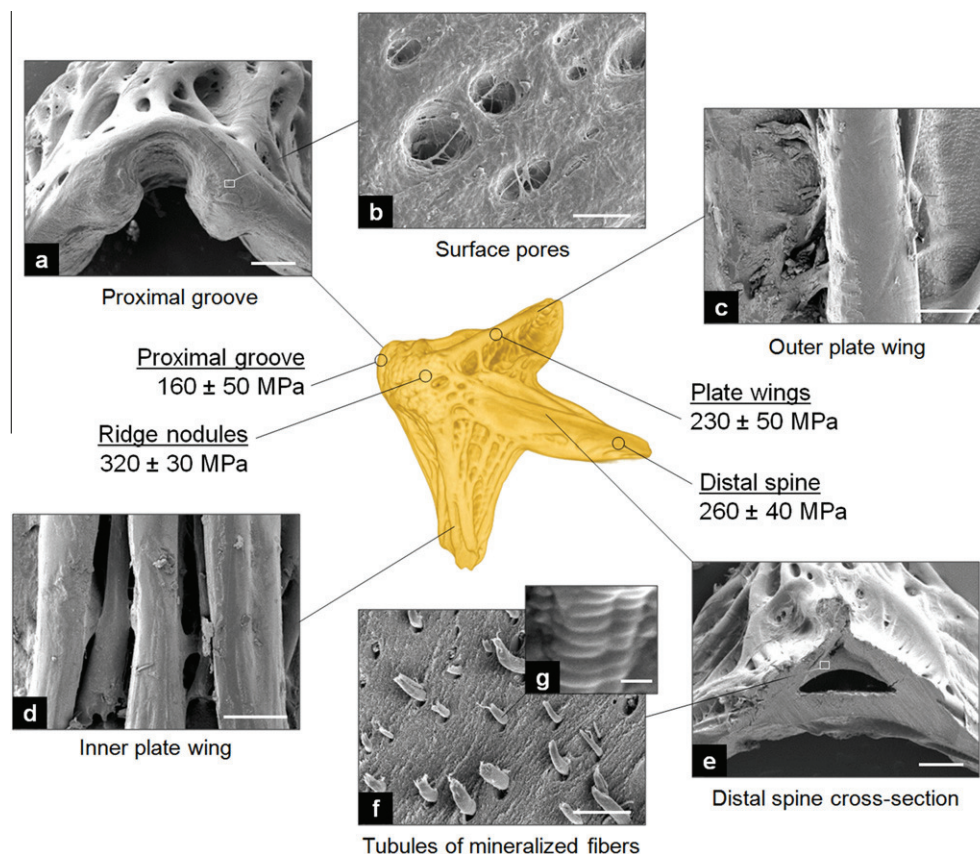
Fig. 6. Structural hierarchy and microhardness distribution of a mature bony plate. (Center) μCT image of a single bony plate, showing the Vickers microhardness at four different locations: proximal groove (160 ± 50 MPa), ridge nodules (320 ± 30 MPa), plate wings (230 ± 50 MPa), and distal spine (260 ± 40 MPa). SEM micrographs: (a) rounded architecture of the proximal groove; (b) surface pores on the proximal groove; (c) reinforcing rod-like strut on the outer plate wing; (d) reinforcing branched struts on the inner plate wing; (e) cross-section of distal spine showing a hollow microchannel; (f) fracture surface of distal spine showing microtubules containing bundles of mineralized organic fibers; (g) mineralized collagen fiber bundle exhibiting characteristic periodicity (~67 nm). Scale bars: (a) 250 μm; (b) 10 μm; (c) 200 μm; (d) 200 μm; (e) 250 μm; (f) 10 μm; (g) 200 nm.

containing bundles of mineralized collagen fibers with a characteristic periodicity of ∼67 nm (Fig. 6g) [26]. Akin to other natural structural materials such as mammalian bones, teeth, antlers, horns and hooves, the directional alignment of structural fibers and the presence of microtubules cause the bony plates to be highly anisotropic, energy-absorbent materials [24]. Collapse of the microtubules under certain loading conditions prevents the buckling of structural fibers and arrests crack propagation. This type of localized failure is an extrinsic toughening mechanism commonly found in bone that protects the integrity of the overall structure [27].

4. Conclusions

The bony-plated armor in the tail of seahorses is a multifunctional device that provides structural support, protection and prehension. Upon compression, the overlapping bony plates slide past each other, allowing the tail to be compressed to nearly 50% its original length before any permanent damage is observed. Even after permanent deformation occurs (>50% deformation), the tail does not exhibit brittle fracture. Instead, it exhibits a plastic response, which is accompanied by local buckling and bending of the bony plates and vertebral struts. This unusual deformation behavior protects the tail segments and central vertebrae from fracture, as the majority of seahorse predators capture their prey by crushing—crabs using claws; rays using crushing plates; sea turtles and birds using beaks [13]. In addition to the impressive structural mechanics of the prehensile appendage, microhardness tests showed a distribution of hardness across a single bony plate that is tailored to specific functions—harder on the outer surface for protection and softer at the overlapping joints for mobility. The unique hierarchical structure–property–function relationships revealed by the seahorse tail may serve as inspiration for future biomimetic devices, such as steerable catheters [12], earthquake-resistant structures, flexible armor, controlled anchoring mechanisms or prehensile robotics.

Acknowledgements

Appendix A. Figures with essential colour discrimination

All figures in this article are difficult to interpret in black and white. The full colour images can be found in the on-line version, at doi: 10.1016/j.actbio.2013.02.045.

References

[1] Chen PY, McKittrick J, Meyers MA. Biological materials: functional adaptations and bioinspired designs. Prog Mater Sci 2012;57:1492–704.
[2] Bar-Cohen Y. Biomimetics: biologically inspired technologies. Boca Raton, FL: Taylor and Francis; 2006.
[3] Lazaris A, Arcidiacono S, Huang Y, Zhou JF, Duguay F, Chretien N, et al. Spider silk fibers spun from soluble recombinant silk produced in mammalian cells. Science 2002;295:472–6.
[4] Vollrath F, Knight DP. Liquid crystalline spinning of spider silk. Nature 2001;410:541–8.
[5] Dickinson MH, Lehmann FO, Sane SP. Wing rotation and the aerodynamic basis of insect flight. Science 1999;284:1954–60.
[6] Ellington CP, van den Berg C, Willmott AP, Thomas ALR. Leading-edge vortices in insect flight. Nature 1996;384:626–30.
[7] Lourie SA, Stanley HF, Vincent ACJ, Hall HJ, Pritchard JC, Casey SP, et al. Seahorses: an identification guide to the world's species and their conservation. London: Project Seahorse; 1999.
[8] Foster SJ, Vincent ACJ. Life history and ecology of seahorses: implications for conservation and management. J Fish Biol 2004;65:1–61.
[9] Consi TR, Seifert PA, Triantafyllou MS, Edelman ER. The dorsal fin engine of the seahorse (Hippocampus sp.). J Morphol 2001;248:80–97.
[10] Ashley-Ross MA. Mechanical properties of the dorsal fin muscle of seahorse (Hippocampus) and pipefish (Syngnathus). J Exp Zool 2002;293:561–77.
[11] Hale ME. Functional morphology of ventral tail bending and prehensile abilities of the seahorse, Hippocampus kuda. J Morphol 1996;227:51–65.
[12] Praet T, Adriaens D, Cauter SV, Masschaele B, Beule MD, Verhegghe B. Inspiration from nature: dynamic modelling of the musculoskeletal structure of the seahorse tail. Int J Numer Methods Biomed Eng 2012:2012.
[13] Kleiber D, Blight LK, Caldwell IR, Vincent ACJ. The importance of seahorses and pipefishes in the diet of marine animals. Rev Fish Biol Fish 2011;21:205–23.
[14] Lin YS, Wei CT, Olevsky EA, Meyers MA. Mechanical properties and the laminate structure of Arapaima gigas scales. J Mech Behav Biomed Mater 2011;4:1145–56.
[15] Chen PY, Lin AYM, McKittrick J, Meyers MA. Structure and mechanical properties of crab exoskeletons. Acta Biomater 2008;4:587–96.
[16] Barthelat F, Li CM, Comi C, Espinosa HD. Mechanical properties of nacre constituents and their impact on mechanical performance. J Mater Res 2006;21:1977–86.
[17] Webb PW, Hardy DH, Mehl VL. The effect of armored skin on the swimming of longnose gar, lepisosteus-osseus. Can J Zool-Rev Can Zool 1992;70:1173–9.
[18] Bruet BJF, Song JH, Boyce MC, Ortiz C. Materials design principles of ancient fish armour. Nat Mater 2008;7:748–56.
[19] Long JH, Hale ME, McHenry MJ, Westneat MW. Functions of fish skin: flexural stiffness and steady swimming of longnose gar Lepisosteus osseus. J Exp Biol 1996;199:2139–51.
[20] Currey JD, Zioupos P, Davies P, Casinos A. Mechanical properties of nacre and highly mineralized bone. Proc Biol Sci 2001;268:107–11.
[21] Zioupos P, Currey JD, Casinos A. Exploring the effects of hypermineralisation in bone tissue by using an extreme biological example. Connect Tissue Res 2000;41:229–48.
[22] Harary G, Tal A. The natural 3D spiral. Comput Graphics Forum 2011;30:237–46.
[23] Valladares S, Planas M. Non-lethal dorsal fin sampling for stable isotope analysis in seahorses. Aquat Ecol 2012;46:363–70.
[24] McKittrick J, Chen PY, Tombolato L, Novitskaya EE, Trim MW, Hirata GA, et al. Energy absorbent natural materials and bioinspired design strategies: a review. Mater Sci Eng C 2010;30:331–42.
[25] Cohen L, Dean M, Shipov A, Atkins A, Monsonego-Ornan E, Shahar R. Comparison of structural, architectural and mechanical aspects of cellular and acellular bone in two teleost fish. J Exp Biol 2012;215:1983–93.
[26] Dorozhkin SV, Epple M. Biological and medical significance of calcium phosphates. Angew Chem Int Ed 2002;41:3130–46.
[27] Launey ME, Buehler MJ, Ritchie RO. On the mechanistic origins of toughness in bone. In: Clarke DR, Ruhle M, Zok F, editors. Annual review of materials research, vol. 40. Palo Alto: Annual Reviews; 2010. p. 25–53.